

# Microwave amplification with nanomechanical resonators

F. Massel,<sup>1\*</sup> T. T. Heikkilä,<sup>1</sup> J.-M. Pirkkalainen,<sup>1</sup> S. U. Cho,<sup>1</sup>  
H. Saloniemi,<sup>2</sup> P. Hakonen,<sup>1</sup> M. A. Sillanpää,<sup>1</sup>

<sup>1</sup> Low Temperature Laboratory, Aalto University,  
P.O. Box 15100, FI-00076 Aalto, Finland

<sup>2</sup>Microsystems and Nanoelectronics, VTT Technical Research Centre of Finland,  
P.O. Box 1000, FI-02044 VTT, Finland

\*To whom correspondence should be addressed; E-mail: francesco.massel@aalto.fi.

**Sensitive measurement of electrical signals is at the heart of modern science and technology. According to quantum mechanics, any detector or amplifier is required to add a certain amount of noise to the signal, equaling at best the energy of quantum fluctuations[1, 2]. The quantum limit of added noise has nearly been reached with superconducting devices which take advantage of nonlinearities in Josephson junctions[3, 4]. Here, we introduce a new paradigm of amplification of microwave signals with the help of a mechanical oscillator. By relying on the radiation pressure force on a nanomechanical resonator[5–7], we provide an experimental demonstration and an analytical description of how the injection of microwaves induces coherent stimulated emission and signal amplification. This scheme, based on two linear oscillators, has the advantage of being conceptually and practically simpler than the Josephson junction devices, and, at the same time, has a high potential to reach quantum limited operation. With a measured signal amplification of 25 decibels and the addition of 20 quanta of noise, we anticipate near**

**quantum-limited mechanical microwave amplification is feasible in various applications involving integrated electrical circuits.**

Since the early days of quantum mechanics, the effect of quantum zero point fluctuations on measurement accuracy has been actively investigated. When measuring a position  $x$  of an object, one necessarily disturbs its subsequent motion by introducing a disturbance to the momentum  $p$ . The imprecision and disturbance are related by the fundamental limit  $\Delta x \Delta p \geq \hbar/2$  owing to the Heisenberg uncertainty principle. A proper compromise between the two leads to the lowest added noise power per unit bandwidth  $\hbar\omega/2$  which equals the quantum fluctuations of the system itself at the signal frequency  $\omega$ . On the other hand, if only one observable is measured, for example position, or a single quadrature such as either amplitude or phase of oscillations, noise in this measurement can be squeezed below the quantum limit at the expense of increased noise in the other quadrature. In this case, the amplifier is said to be phase-sensitive.

While most modern transistors operate several orders of magnitude above the fundamental noise limit, superconducting Josephson junction parametric amplifiers[3, 4, 8, 9], working near the absolute zero of temperature, have found uses at the level of only a few added quanta at microwave frequencies. Approaching the quantum limit with a mechanical amplifier has remained fully elusive, moreover, there is little work whatsoever on amplifying electrical signals by mechanical means[10], foremost due to the typically small electromechanical interaction. In this work, we describe a way to approach quantum-limited microwave amplification, now with a mechanical device. Our system consists of a mechanical resonator affected by radiation pressure forces due to an electromagnetic field confined in a lithographically patterned thin-film microwave cavity. Depending on the configuration, it is capable of either phase-sensitive, or phase-insensitive amplification.

Our system of two coupled linear oscillators forms possibly the simplest realization of quan-

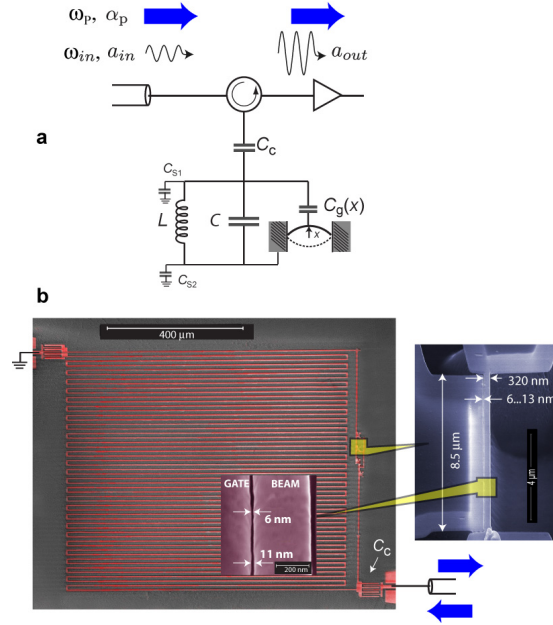


Figure 1: **Schematics of the electromechanical microwave amplification.** **a**, The movable capacitance of the micromechanical resonator is in parallel to the cavity, represented by its lumped element equivalent model. The input microwave field is decomposed into a blue-detuned pump coherent field  $\alpha_p$  at the frequency  $\omega_p$ , and a signal (frequency  $\omega_{in}$ ) + noise  $a_{in} = \alpha_{in} + \delta a_{in}$ . The output signal  $a_{out}$  describes the amplified input signal. **b**, Image of the device is dominated by the meandering high-impedance cavity (false color in red), resonating at  $\omega_c/(2\pi) = 6.982$  GHz. It is connected to coaxial cables via a coupling capacitor for operations. The micromechanical beam resonator (frequency  $\omega_m/(2\pi) = 32.5$  MHz) couples the ends of the meander via the protrusions from either end, and through an 6...15 nm nanometer vacuum gap[19] (right, and inset).

tum amplification of external signals. The analysis connects directly to the potential quantum behavior of macroscopic mechanical objects[11–13], and the emergence of macroscopic phenomena from the quantum-mechanical laws governing nature on a microscopic scale. Besides fundamental significance, the use of mechanical objects as a building block of low-noise amplification might be advantageous over electrical realization because of the possibility of obtaining an elementary physical structure. Ultimately, these devices can be made with single-crystalline resonant beams or membranes.

More specifically, our system involves an on-chip microwave cavity parametrically inter-

acting with a micromechanical resonator [14–16], so that the mechanical motion couples to the frequency of the cavity (see Fig. 1). In a similar setup, freezing of the mechanical Brownian motion is expected to take place due to the conversion of mechanical vibrations into electromagnetic radiation [6, 16–18]. The interaction gives rise to energy  $H_{\text{int}} = -\hbar g (n_c + \frac{1}{2}) x$ , where  $n_c$  is the number of coherently driven photons in the cavity,  $g = (\omega_c/2C)\partial C_g/\partial x$  is the electromechanical interaction, and  $x$  is the displacement. The cavity is driven with a strong microwave tone  $\alpha_p$  (hereafter denoted as the pump) having a frequency  $\omega_p \sim \omega_c + \omega_m$  which exceeds the resonant frequency  $\omega_c$  of the cavity approximately by the mechanical frequency  $\omega_m$ , see Fig. 2. The condition  $\omega_p > \omega_c$  is referred to as blue-detuning for the pump with respect to the cavity resonant frequency, as opposed to the red-detuning condition  $\omega_p < \omega_c$  encountered in the sideband cooling regime both for electro- and optomechanical systems [6, 16]. On the red-detuned side, the microwave/mechanics coupling generates a net energy transfer from the mechanical degrees of freedom into the cavity, hence effectively leading to the cooling of the mechanics. Contrarily, on the blue-detuning side, the microwave pump gives rise to an energy transfer into the mechanical degrees of freedom. This situation can be pictured with the relevant energy levels as in Fig. 2b: A weak probe signal near the frequency  $\omega_c$  induces stimulated emission of microwave photons, effectively leading to amplification of the probe signal.

Some details of our actual device are depicted in Fig. 1b. The micromechanical resonator consists of an aluminum micromechanical beam resonator having the length  $8.5 \mu\text{m}$ , width  $320 \text{ nm}$ , which yield the frequency of the lowest flexural mode  $\omega_m/(2\pi) = 32.5 \text{ MHz}$  and linewidth  $\gamma_m \sim 500 \dots 1200 \text{ Hz}$  (depending on temperature). Via an ultranarrow vacuum gap [19], the displacement affects the end-to-end capacitance of the cavity, which is a superconducting microstrip resonator having the natural frequency  $\omega_c \gg \omega_m$  and linewidth  $\gamma_c$ . In order to obtain the largest electromechanical coupling, the device was fabricated on a fused silica substrate. This material has a low dielectric constant ( $\epsilon_r \simeq 4$ ), as compared to, for instance, frequently

used silicon ( $\epsilon_r \simeq 12$ ), which contributes to minimizing the stray capacitance  $C \simeq 18$  fF of the cavity. These measures, and the remaining equivalent parameters ( $L = 21$  nH,  $C_{S1} = 6$  fF,  $C_{S2} = 12$  fF,  $C_g = 0.6$  fF, see Fig. 1a), create a strong electromechanical coupling  $g/(2\pi) \simeq 40$  Hz per phonon, or, in frequently used units,  $g/(2\pi) = 1.8$  MHz/nm. An interdigital coupling capacitor  $C_c \sim 6$  fF results in the external damping rate  $\gamma_E/(2\pi) = 4.8$  MHz. The total cavity linewidth is  $\gamma_c = \gamma_E + \gamma_I \simeq (2\pi) \times 6.2$  MHz, where  $\gamma_I/(2\pi) = 1.4$  MHz is due to internal losses.

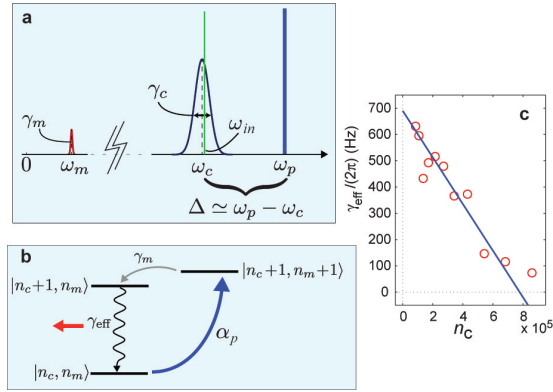


**Figure 2: Amplification mechanism.** **a**, Explanation of the various frequencies involved: The cavity is driven by a (pump,  $\alpha_p$ ) coherent field oscillating at  $\omega_p = \omega_c + \Delta$ , where  $\omega_c$  is the cavity resonant frequency, and  $\Delta \simeq \omega_m \ll \omega_c$ . The weak input signal  $a_{in}$  to be amplified is applied near the cavity resonance, such that  $\omega_{in} = \omega_p - \omega_m$ . **b**, The physics of the electromechanical amplifier can be intuitively understood by considering a block of three energy levels in the system. The (blue-detuned) pump  $\alpha_p$  induces a transition between a state characterized by  $n_c$  cavity photons and  $n_m$  mechanical quanta and a state with  $n_c + 1$  and  $n_m + 1$ . A key role in the amplification process is played by the effective damping  $\gamma_{eff}$ , which in the simplified scheme presented here represents the effective lifetime for the cavity photons, thus modelling the parametric-down conversion of the pump photons to the cavity resonant frequency. **c**, The damping decreases towards a higher pump field, while below  $\gamma_{eff} = 0$ , instability and parametric oscillations take place. The circles are fitted from the measured mechanical peak in the output spectrum, and the solid line is theory.

The theoretical framework suitable for description of the amplification is closely related to the methodology used to describe the sideband cooling in optomechanical systems [17, 18, 20–23]. We describe the system in terms of quantum Langevin equations with the aim of

analyzing the effect of the pumping on the signal, and especially to detail the effects of different types of fluctuations coupling to the system. The latter are caused by the quantum and thermal fluctuations related to the input signal, the cavity, and the mechanical resonator. In general, the parametric coupling between the cavity and the mechanical resonator gives rise to the possibility of squeezing [24, 25], and hence to back-action evading measurements.

The detailed theoretical analysis (see supplementary information) gives the explicit value of the gain in each preferred quadrature  $\mathcal{G}_x$ ,  $\mathcal{G}_y$  and the average gain  $\mathcal{G}_{av} = \frac{1}{2}(\mathcal{G}_x + \mathcal{G}_y)$ . The expression for the gains are well approximated by

$$\mathcal{G}_{x,y} = 4 |\Gamma_M(\omega)|^2 \left( \frac{\gamma_E}{\gamma_c} \right)^2 \left( \sqrt{1 + \left( \frac{\gamma_c}{4\Delta} \right)^2} \pm \frac{\gamma_c}{\Delta} \right)^2, \quad (1)$$

where the upper (lower) sign corresponds to  $\mathcal{G}_x$  ( $\mathcal{G}_y$ ).

The key role in the microwave amplification is played by the effective mechanical damping  $\gamma_{\text{eff}} = \gamma_m - \delta\gamma_{\text{eff}}(\omega, n_c)$  (see Fig. 2c and supplementary information). The value of  $\delta\gamma_{\text{eff}}$  can be tuned by the pump. In particular, blue-detuned drive corresponds to a sizable reduction of the mechanical damping which is directly related to the signal amplification mechanism described by the factor  $\Gamma_M(\omega) = (\omega_m^2 - \omega^2 - i\gamma_m\omega) / (\omega_{\text{eff}}^2 - \omega^2 - i\gamma_{\text{eff}}\omega)$ , where  $\omega_{\text{eff}} \simeq \omega_m$ . Equation (1) and the definition of  $\gamma_{\text{eff}}$  allow to establish the optimal value for the pumped occupancy as  $n_{c,\text{crit}} = \gamma_c\gamma_m / (4g^2x_0^2)$  associated with the maximum gain  $\mathcal{G}_{av}(\omega = \omega_m) \simeq 4(4\Delta/\gamma_c)^2$ . Above this threshold,  $\gamma_{\text{eff}} \rightarrow 0$ , and the coupled system becomes unstable [5, 7, 26, 27].

Indicated by the unequal  $\mathcal{G}_x$  and  $\mathcal{G}_y$ , the amplifier will portray a variable amount of squeezing. In particular, in the so-called good cavity limit  $\frac{\gamma_c}{\Delta} \ll 1$  used in the present experiment, the squeezing is expected to be insignificant, and the amplifier is hence behaving as a typical phase-insensitive amplifier characterized by the average gain  $\mathcal{G}_{av}$ . However, it is noteworthy that by varying the parameters towards the bad cavity limit  $\frac{\gamma_c}{\Delta} \gg 1$ , one may achieve strong

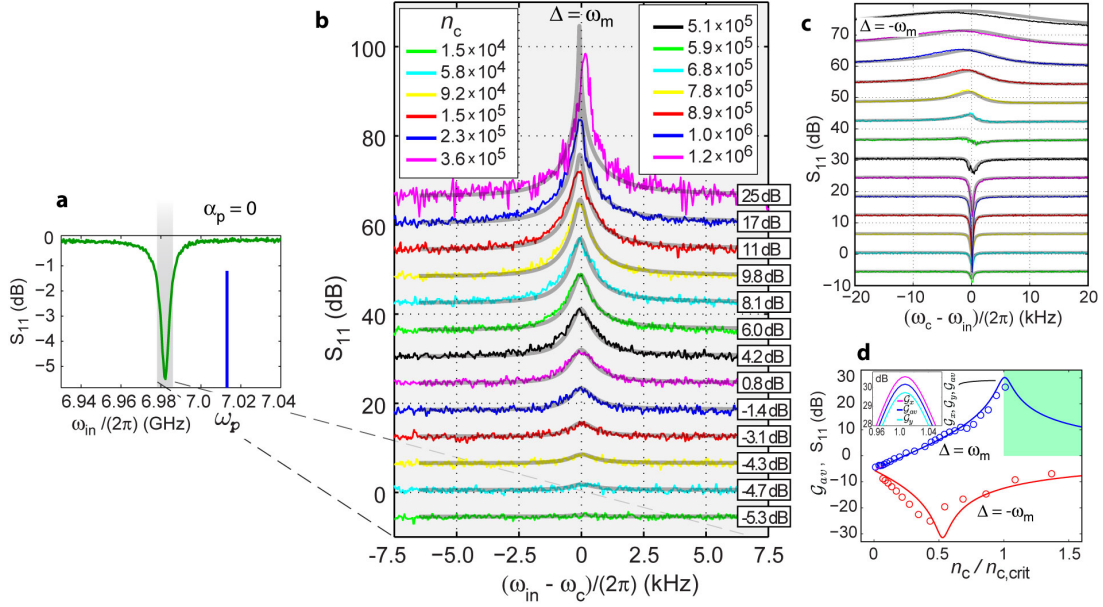


Figure 3: **Amplifier gain.** **a**, Measured reflection magnitude of the signal microwave over a large span about the cavity resonance without applying the pump. **b**, Measured gain (colored lines) in a narrow window (schematically indicated by gray in A) for the pump occupancy  $n_c$  increasing by 2 dB per curve from bottom to top. The curves are displaced vertically for clarity by 3 dB. The baseline of each curve roughly corresponds to the cavity absorption of -5.5 dB. The maximum gain is quoted for each curve. The gray curves are theoretical predictions for the gain  $\mathcal{G}_{av}$  averaged over quadratures. **c**, As panel B, but with *red* detuned pumping. Here, de-amplification of the signal field (sharp dip) is observed.  $n_c$  increases by 2 dB per curve from bottom ( $4.6 \times 10^4$ ) to top. **d**, Calculated average gain (at  $\omega_p - \omega_m$ ), and the quadrature gains  $\mathcal{G}_x, \mathcal{G}_y$  (inset) as a function of the scaled cavity occupancy. The blue traces correspond to amplification ( $\Delta > 0$ ), and red to de-amplification ( $\Delta < 0$ ). The shaded region is the unstable regime (see text). The experimental points are extracted from B and C.

squeezing and, consequently, noise-free amplification in one quadrature.

We used a dilution refrigerator with temperature stabilized between 350...25 mK in order to carry out the measurements. The pump and signal tones are combined at room temperature using a power splitter. Inside the cryostat, the incoming irradiation is attenuated by  $43 \pm 1.5$  dB. The uncertainty in the cryogenic attenuation sets the relatively large error bars for  $n_c$ . The signals reflected from the device chip are directed towards conventional cryogenic amplifier. Following amplification, we used a sharp low-pass filter to remove the strong pump microwave, since we only consider the signal frequency in the processing. The signal is recorded with a vector network analyzer, or, for noise measurements, fed into a spectrum analyzer. Although it is possible to distinguish the different quadrature gains  $\mathcal{G}_x, \mathcal{G}_y$ , for the moment we only consider the phase-insensitive gain  $\mathcal{G}_{av}$ . More details of the practical setup are given in the supplementary information.

At the lowest pump power  $n_c \ll n_{c,crit}$ , we observe an attenuation of the reflected signal according to the cavity absorption at the applied *signal* frequency  $\omega_{in} \sim 6.82$  GHz, for instance,  $\sim -6$  dB around  $\omega_{in} \sim \omega_c$  (Fig. 3a). Towards higher  $n_c$ , a mechanical peak at  $\omega_p - \omega_{in} \simeq \omega_m$  indicates a decreased absorption. A vanishing absorption is observed when  $2\gamma_m/\gamma_{eff} \sim \gamma_E/\gamma_c$ , i.e., when reduced damping balances external losses. This marks an onset of a type of electromechanically induced microwave transparency. Earlier work on the effect [28, 29] used the opposite red-detuned pump conditions. Blue pumping, on the other hand, has the capability of transferring energy to the cavity frequency, and therefore, we observe also amplification of the signal tone, Fig. 3b.

The theoretical prediction, overlaid on the experimental data in Fig. 3b, shows a remarkable agreement with the measurement, with the only adjustable parameter being  $n_c$ , whose values, nevertheless, are independently known within a factor of 2. The maximum gain of 26 dB is observed close to the instability, however, with markedly increased amount of fluctuations,

typical of parametric systems. The useful range of gain where noise is not increased, is up to about 15 dB in this measurement. The operation frequency of the amplifier may be tuned roughly by the amount of the cavity linewidth by detuning the pump slightly off from the exact blue sideband condition. While the data was measured with a small input signal corresponding to about 0.3 signal photons in cavity, a favorable property of the mechanical amplification is its high dynamic range, namely, amplification is observed at least up to  $10^4$  signal photons. This high power handling capability is in striking contrast to the Josephson devices which work in the single-quantum regime.

We can also confirm the theory predictions by inverting the pump frequency to the red sideband, i.e.,  $\Delta = -\omega_m$ , see Fig. 3c. In analog to the enhanced damping under these conditions leading to sideband cooling, we observe de-amplification of the input signal. At even stronger pump  $n_c > n_{c,\text{crit}}$ , decreased absorption indicates that the eigenmode splitting [29] starts to set in. The observed gains (Fig. 3d) as a function of the pumped occupancy are in a good agreement with theory.

Finally, an amplifier should be characterized by its added noise which is commonly referred to the input signal. Because of its simple structure, we expect the mechanical amplifier to be less influenced by the strong  $1/f$  electrical flicker noise typical of nonlinear transistor or Josephson junction devices. What remain as noise sources are thermal fluctuations, and, ultimately, quantum fluctuations in the number of quanta of both cavity and the mechanics. In the case of the optimal gain, the quadrature-averaged added noise at the cavity frequency is

$$\begin{aligned} n_{\text{add}} &= \frac{\gamma_I}{\gamma_c} \left( n_c^T + \frac{1}{2} \right) + \frac{\gamma_c}{\gamma_E} \left( n_m + \frac{1}{2} \right) \\ &\geq \frac{1}{2} \left[ 1 - (\mathcal{G}_x \mathcal{G}_y)^{-1/2} \right] \simeq \frac{1}{2}. \end{aligned} \quad (2)$$

Here,  $n_c^T$  and  $n_m$  represent the finite number of cavity photons associated with the internal losses, and the number of mechanical quanta due to the thermal fluctuations in the mechanical bath, respectively. The quantum limit  $n_{\text{add}} = 1/2$  with large gain may thus be reached if

information is not lost inside the system, that is, if external dissipation of the cavity related to the measurement dominates over internal losses. While in cryogenic experiments typically  $n_c^T \simeq 0$  due to gigahertz-range cavity frequencies, standard mechanical frequencies  $\omega_m/(2\pi) \lesssim 50$  MHz tend to pose a practical limit for noise  $n_{\text{add}} > n_m \gtrsim 10$ .

We measured the added noise by comparing it to a known noise source. Here, the noise floor is set by the effective noise temperature of the system, approximately 6...7 K. We worked at a temperature of 30 mK, and used a weak input signal as a marker (see supplementary information). We obtained a slight 0.6 dB improvement to the signal-to-noise ratio, which corresponds to 20 added noise quanta at the signal frequency of 7 GHz. This finding agrees remarkably well with the ideal prediction equaling the thermal phonon number, and shows that no extra noise appeared in the process. Hence, an even further improved performance closer to the quantum limit looks promising.

We have shown that interaction of a micromechanical device and radiation pressure can be used for amplifying weak electrical signals. This finding opens up new perspectives for an alternative to the conventional electrical microwave amplifiers, and may facilitate radiation detection in the difficult terahertz band. From a theoretical point of view, the setup represents one of the simplest realizations of a quantum amplifier leading to operation at the noise limit set by the Heisenberg uncertainty principle. In the first proof-of-principle device, the mechanical amplifier showed no extra added noise beyond that predicted by the ideal theoretical model. For a practical application, the frequency band can be made variable over a larger span by using tunable cavities[3, 30]. An even higher electromechanical coupling, for instance, by the use of piezoelectric materials[13], can allow for an increase of the band via an engineered increase of damping. At a higher mechanical frequency in the GHz range, or with the help of pre-cooling by opposite pumping at even high temperatures, we can foresee near-quantum limited operation.

**Acknowledgements** We would like to thank Sorin Paraoanu for useful discussions. This

work was supported by the Academy of Finland, and by the European Research Council (grants No. 240362-Heatronics and 240387-NEMSQED) and EU-FP7-NMP-246026.

**Author Contributions** F.M. and T.H. developed the theory. J.-M.P. and S.U.C. contributed to design and fabrication of the samples, and cryogenic setup. H.S. made the samples. P.H. and M.S. designed the experimental setup. M.S. initiated the work and carried out the measurements.

**Author Information** The authors declare no competing financial interests. Correspondence and requests for materials should be addressed to F.M. (francesco.massel@aalto.fi).

## References

- [1] Caves, C. M. Quantum limits on noise in linear-amplifiers. *Phys. Rev. D* **26**, 1817–1839 (1982).
- [2] Haus, H. A. *Electromagnetic Noise and Quantum Optical Measurements (Advanced Texts in Physics)* (Springer, 2000).
- [3] Castellanos-Beltran, M. A., Irwin, K. D., Hilton, G. C., Vale, L. R. & Lehnert, K. W. Amplification and squeezing of quantum noise with a tunable Josephson metamaterial. *Nat. Phys.* **4**, 929–931 (2008).
- [4] Bergeal, N. *et al.* Phase-preserving amplification near the quantum limit with a Josephson ring modulator. *Nature* **465**, 64–68 (2010).
- [5] Braginsky, V. B., Strigin, S. E. & Vyatchanin, S. P. Parametric oscillatory instability in Fabry-Perot interferometer. *Phys. Lett. A* **287**, 331–338 (2001).
- [6] Metzger, C. H. & Karrai, K. Cavity cooling of a microlever. *Nature* **432**, 1002–1005 (2004).

- [7] Kippenberg, T. J., Rokhsari, H., Carmon, T., Scherer, A. & Vahala, K. J. Analysis of radiation-pressure induced mechanical oscillation of an optical microcavity. *Phys. Rev. Lett.* **95**, – (2005).
- [8] Yurke, B. *et al.* Observation of 4.2-K equilibrium-noise squeezing via a Josephson-parametric amplifier. *Phys. Rev. Lett.* **60**, 764–767 (1988).
- [9] André, M. O., Mück, M., Clarke, J., Gail, J. & Heiden, C. Radio-frequency amplifier with tenth-kelvin noise temperature based on a microstrip direct current superconducting quantum interference device. *Appl. Phys. Lett.* **75**, 698–700 (1999).
- [10] Raskin, J. P., Brown, A. R., Khuri-Yakub, B. T. & Rebeiz, G. M. A novel parametric-effect MEMS amplifier. *J. Microelectromech. S.* **9**, 528–537 (2000).
- [11] Leggett, A. J. Testing the limits of quantum mechanics: motivation, state of play, prospects. *J. Phys-Condens. Mat.* **14**, R415–R451 (2002).
- [12] Marshall, W., Simon, C., Penrose, R. & Bouwmeester, D. Towards Quantum Superpositions of a Mirror. *Phys. Rev. Lett.* **91**, 130401 (2003).
- [13] O’Connell, A. D. *et al.* Quantum ground state and single-phonon control of a mechanical resonator. *Nature* **464**, 697–703 (2010).
- [14] Regal, C. A., Teufel, J. D. & Lehnert, K. W. Measuring nanomechanical motion with a microwave cavity interferometer. *Nat. Phys.* **4**, 555–560 (2008).
- [15] Sillanpää, M. A., Sarkar, J., Sulkko, J., Muhonen, J. & Hakonen, P. J. Accessing nanomechanical resonators via a fast microwave circuit. *Appl. Phys. Lett.* **95**, 011909 (2009).
- [16] Rocheleau, T. *et al.* Preparation and detection of a mechanical resonator near the ground state of motion. *Nature* **463**, 72–75 (2010).

- [17] Marquardt, F., Chen, J. P., Clerk, A. A. & Girvin, S. M. Quantum theory of cavity-assisted sideband cooling of mechanical motion. *Phys. Rev. Lett.* **99**, 093902 (2007).
- [18] Wilson-Rae, I., Nooshi, N., Zwerger, W. & Kippenberg, T. J. Theory of ground state cooling of a mechanical oscillator using dynamical backaction. *Phys. Rev. Lett.* **99**, 093901 (2007).
- [19] Sulkko, J. *et al.* Strong Gate Coupling of High-Q Nanomechanical Resonators. *Nano Lett.* **10**, 4884–4889 (2010).
- [20] Mancini, S. & Tombesi, P. Quantum-noise reduction by radiation pressure. *Phys. Rev. A* **49**, 4055–4065 (1994).
- [21] Genes, C., Vitali, D., Tombesi, P., Gigan, S. & Aspelmeyer, M. Ground-state cooling of a micromechanical oscillator: Comparing cold damping and cavity-assisted cooling schemes. *Phys. Rev. A* **77**, 033804 (2008).
- [22] Walls, D. F. & Milburn, G. J. *Quantum Optics* (Springer, Berlin, 2007).
- [23] Clerk, A. A., Devoret, M. H., Girvin, S. M., Marquardt, F. & Schoelkopf, R. J. Introduction to quantum noise, measurement, and amplification. *Rev. Mod. Phys.* **82**, 1155–1208 (2010).
- [24] Rugar, D. & Grütter, P. Mechanical parametric amplification and thermomechanical noise squeezing. *Phys. Rev. Lett.* **67**, 699–702 (1991).
- [25] Woolley, M. J., Doherty, A. C., Milburn, G. J. & Schwab, K. C. Nanomechanical squeezing with detection via a microwave cavity. *Phys. Rev. A* **78**, 062303 (2008).
- [26] Carr, D. W., Evoy, S., Sekaric, L., Craighead, H. G. & Parpia, J. M. Parametric amplification in a torsional microresonator. *Appl. Phys. Lett.* **77**, 1545–1547 (2000).

- [27] Arcizet, O., Cohadon, P. F., Briant, T., Pinard, M. & Heidmann, A. Radiation-pressure cooling and optomechanical instability of a micromirror. *Nature* **444**, 71–74 (2006).
- [28] Weis, S. *et al.* Optomechanically Induced Transparency. *Science* **330**, 1520–1523 (2010).
- [29] Teufel, J. D. *et al.* Circuit cavity electromechanics in the strong-coupling regime. *Nature* **471**, 204–208 (2011).
- [30] Palacios-Laloy, A. *et al.* Tunable resonators for quantum circuits. *J. Low Temp. Phys.* **151**, 1034–1042 (2008).

# Microwave amplification with nanomechanical resonators: Supplementary Information

F. Massel,<sup>1\*</sup> T. T. Heikkilä,<sup>1</sup> J.-M. Pirkkalainen,<sup>1</sup> S. U. Cho,<sup>1</sup>  
H. Saloniemi,<sup>2</sup> P. Hakonen,<sup>1</sup> M. A. Sillanpää,<sup>1</sup>

<sup>1</sup> Low Temperature Laboratory, Aalto University,  
P.O. Box 15100, FI-00076 Aalto, Finland

<sup>2</sup>Microsystems and Nanoelectronics, VTT Technical Research Centre of Finland,  
P.O. Box 1000, FI-02044 VTT, Finland

\*To whom correspondence should be addressed; E-mail: francesco.massel@aalto.fi.

## 1 Description of the experiment

### 1.1 Sample fabrication

In order to minimize the stray capacitance  $C$  of the cavity, the device was fabricated on a fused silica ( $\text{SiO}_2$ , glass) substrate, which has a low dielectric constant ( $\epsilon_r \simeq 4$ ), as compared to, for instance, silicon ( $\epsilon_r \simeq 12$ ).

Both the cavity and the structures for the beam were made in a single e-beam lithography step, followed by evaporation of 150 nm aluminum. In order to suspend the beams, the substrate was etched by the use of HF vapor etcher, for 500 seconds at a pressure of 150 torr. The use of HF vapor instead of liquid oxide etchant is necessary in order to avoid damaging the aluminum film. The depth of the roughly isotropic etch was about 700 nm.

The mechanical beams were defined by Focused Ion Beam (FIB) etching, as in Ref. [1]. In order to create uniform 9-12 nm vacuum slit over the whole length  $L = 8.5 \mu\text{m}$  of the beam, we

used low gallium ion currents of 1.5 pA and 75% exposure overlap in a single cutting pass. In order to avoid charge accumulation due to the insulating substrate, all the structures were kept galvanically short-circuited and connected to ground until the very end of fabrication.

## 1.2 Cavity design and characterization

The cavity was designed and fabricated such that it would have a high critical current in order to enable a high drive  $n_c \gtrsim 10^8$ , and as small stray capacitance  $C$  as possible. The first requirement suggests to fabricate it in a single lithography step. The low dielectric constant ( $\epsilon_r \simeq 4$ ) of the substrate contributes to a low stray capacitance, moreover, the roughly isotropic release etch for the beam, which partially suspended also the cavity, finally contributed such that  $\epsilon_r \sim 3$  for the final structure.

The cavity design (Fig. 1A) is a 2 microns wide, 45 mm long meandering microstrip floating from both ends, and the mode we are using is the lowest mode of the structure which roughly corresponds to  $\lambda/2$  resonance in a typical transmission line resonator (where the cross-coupling between adjacent meanders is negligible). There are similar interdigital coupling capacitors  $C_c \simeq 6$  fF in both ends, however, only one of them is used, while the other one is shorted to ground. In order to deduce the value of  $C$ , and the validity of the parallel  $LC$  model in the somewhat complicated structure whatsoever, we made electromagnetic simulations with ideal inductor and capacitor components  $C_g$  and  $L_g$  inserted between the open ends of the meander, see Fig. 1a,b. By inspecting how their values affect the mode frequency, one can extract  $C$  and  $L$  from  $\omega_c = [(L||L_g)(C + C_g)]^{-1/2}$  (ignoring the effects of  $C_c$ ,  $C_{S1}$  and  $C_{S2}$ ). The effective stray capacitance, which sets the coupling energy, is then roughly the parallel sum  $C + C_c \simeq 24$  fF.

The values of  $C_S$  are further determined from a lumped element circuit simulation, by comparing to the measured reflection parameters. From the experiment, we obtain the FWHM of the

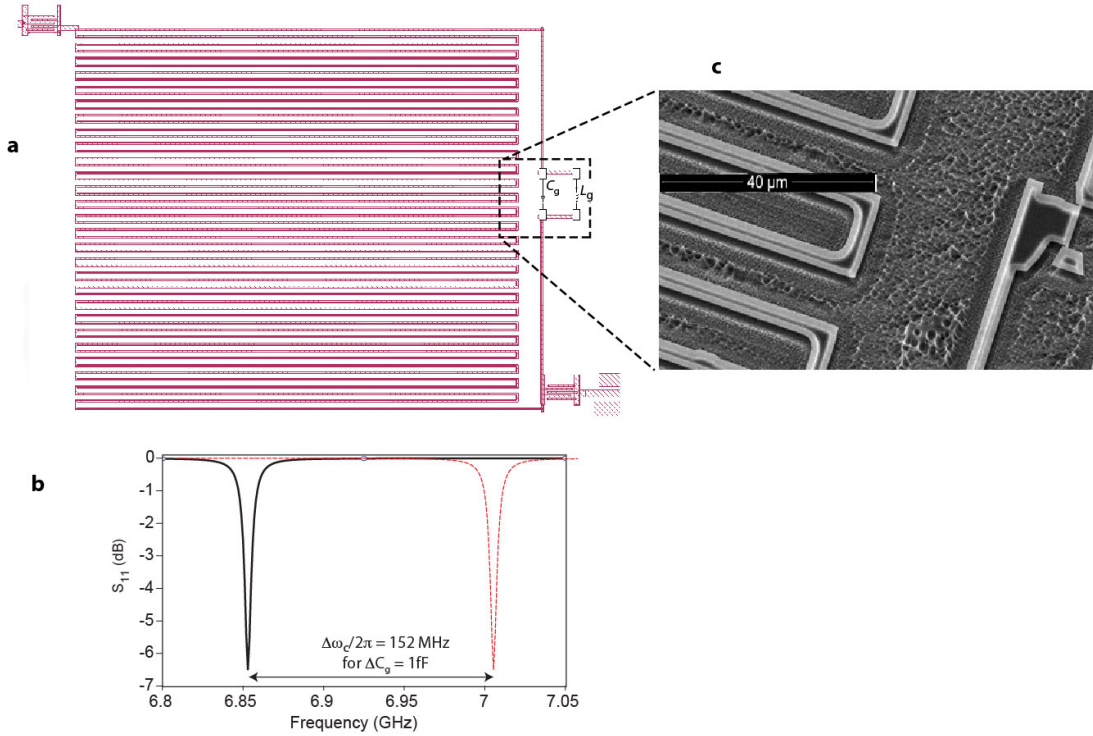


Figure 1: **Design for the cavity.** **a**, Simulation drawing for the meandering cavity structure, with ideal circuit components inserted between the open ends; **b**, change of the cavity resonance for 1 fF change of  $C_g$ ; **c**, micrograph showing the clamped beam and part of the cavity. The roughly isotropic etch causes about 700 nm undercut also for the cavity.

$S_{11}$  magnitude of  $(2\pi) \times 6.0$  MHz, and the maximum absorption at resonance of -5.5 dB. Note that there is no accurate simple relation for obtaining  $\gamma_c = \omega_c/Q_c$  from the *reflection* measures. Instead, it holds for the *driven response*  $\chi(\omega)$  of the *LC* circuit that FWHM  $\Delta\omega_c = \sqrt{3}\gamma_c$ . We determine  $\Delta\omega_c$  from the lumped element simulation: internal losses, modeled by a resistor, are first adjusted to match the measured absorption. The driven response function, including  $\Delta\omega_c$ , is then given by, for example, the current  $i_L$  flowing through  $L$ , as a function of frequency:

$$\chi(\omega) \equiv i_L(\omega)/i_L(\omega_c) = \frac{\gamma_c \omega_c}{\sqrt{\gamma_c^2 \omega^2 + (\omega^2 - \omega_c^2)^2}} \quad (1)$$

This way, we obtain  $\Delta\omega_c \simeq (2\pi) \times 12.2$  MHz, and finally an estimate  $\gamma_{c,S_{11}} = (2\pi) \times 7.0$  MHz. The ratio of internal and external dissipation  $\gamma_I/\gamma_E \simeq 3.4$  is determined by the resonance

absorption.

In section 1.4, using pump detuning measurement, we make the most accurate measurement to yield the final numbers  $\gamma_c = (2\pi) \times 6.2$  MHz,  $\gamma_I = (2\pi) \times 1.4$  MHz and  $\gamma_E = (2\pi) \times 4.8$  MHz, which come close to those deduced here.

The cavity number of quanta  $n_c$  at a given detuning is given by  $n_c(\omega)/n_c(\omega_c) = \chi^2(\omega)$ , and  $n_c(\omega_c) = Li_L(\omega_c)^2$ . The current response  $i_L(\omega_c)$  at a given input power is again obtained from lumped element simulation.

### 1.3 Cryogenic setup

The experiments were carried out in a dilution refrigerator down to 25 mK temperatures. The pump and probe signals are combined at room temperature using a power splitter. Before the signals enter the cryostat, a sharp high-pass filter at room temperature is used to cut the phase noise of the generators near the cavity frequency. This filter provides 50 dB more attenuation at the cavity frequency than at the blue sideband. Without proper filtering, the phase noise would reflect from the cavity, and appear as extra added noise of tens of quanta. Inside cryostat, the incoming signals are attenuated by  $43 \pm 1.5$  dB. The uncertainty in the cryogenic attenuation sets the relatively large error bars for  $n_c$ . Thermal noise emanating from higher temperatures is estimated to contribute less than 0.1 quanta of thermal occupancy into the cavity, and is thus a negligible contribution to the total noise. The entire setup is described in Fig. 2.

The signals reflected from the amplifier chip are directed to the cryogenic amplifier which has a high input compression point of -20 dBm which allows for using high pump powers without problems of amplifier saturation. The amplifier has a noise temperature  $\sim 4$  Kelvins. In addition, there is attenuation of 2...2.5 dB due to circulators and cables between the sample and the amplifier. The effective noise temperature, which sets the signal-to-noise ratio, is then 6...7 K.

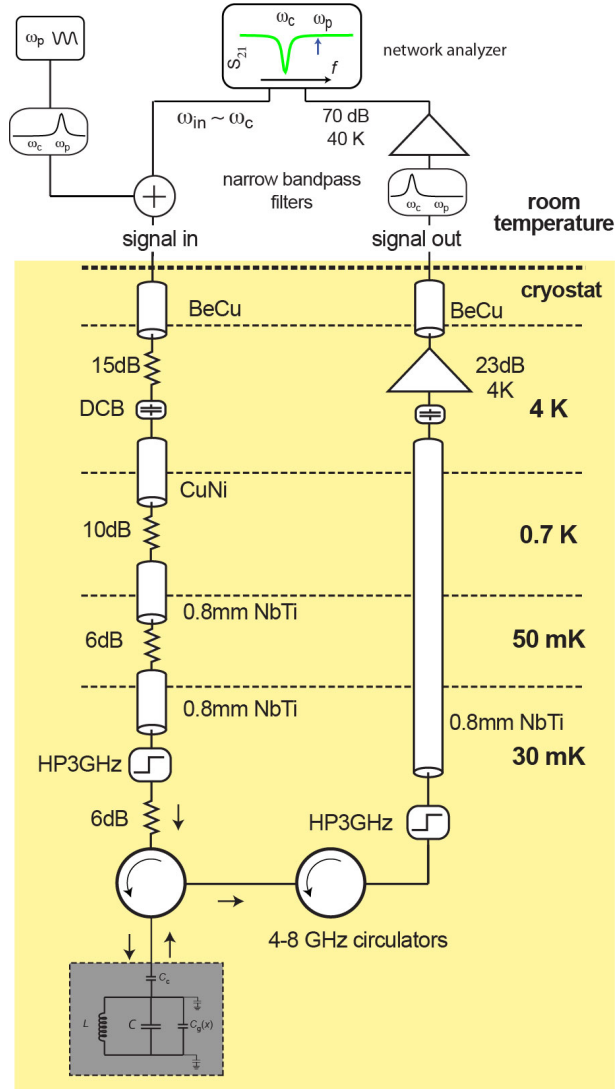


Figure 2: **Setup for electronics and the microwave cabling** inside the dilution refrigerator for the electromechanical amplifier experiment. Inside the dilution cryostat, we use beryllium copper (BeCu), copper nickel (CuNi), and niobium titanium (NbTi) coaxial cables. Inner-pin DC-blocks (DCB), and high-pass filters (HP) are used to reduce heat leak. Back at room temperature, the pump is blocked from the output signal. After further amplification, the signal microwave is recorded coherently in a network analyzer.

## 1.4 Characterization of the electromechanical system

In order to establish a good understanding of the basic behavior of the electromechanical system, we determined its parameters independently of the amplification measurements.

For determining the electromechanical coupling energy  $g = \frac{w_c}{2C} \frac{\partial C_g}{\partial x}$ , we used the value for  $C \simeq 24$  fF as obtained in section 1.2. Moreover,  $\frac{\partial C_g}{\partial x} \simeq 13$  nF/m is estimated from the dimensions of the beam and the vacuum slit. We get  $g = (2\pi) \times 1.8$  MHz/nm, which corresponds to shift of the cavity frequency of 40 Hz per phonon. Similarly as previously done in Refs. [2, 3], we made measurements where the pump frequency or power is varied near the blue sideband. This alters the optical spring effect which can be compared to the theory for shifts for frequency and damping, Eqs. 26, 27 in the supporting online text. The effective mechanical frequency may be read from the position of mechanical sideband, more precisely, from the departure of this peak from the pump frequency.

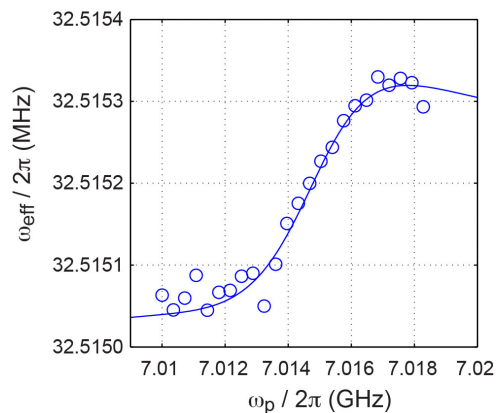


Figure 3: **Characterization of the electromechanical system via the optical spring effect.** The incident microwave power was kept constant such that at the blue sideband frequency,  $n_c \sim 5.3 \times 10^5$ .

In Fig. 3 we compare the measured effective mechanical frequency to the theory. Corresponding plots for the damping are shown in the main text in Figs. 2A and 3D. The best fit is obtained with  $\gamma_c = 6.2$  MHz. This value differs 10 % from that deduced from the  $S_{11}$  measurement. We consider this value of  $\gamma_c$  the most reliable, and will use it in the rest of the paper.

The values of  $n_c$  we get from these fits are about 30 % smaller than those from independent estimates based on the input attenuation and cavity response. We attribute this difference to the

somewhat inaccurately known cryogenic attenuation, which has a sensitive effect on  $n_c$ . We adjust the scale of  $n_c$  according to these fits, and quote the adjusted values in the paper. For instance, a useful fixed point is the instability point, which is expected according to theory at  $n_c \sim 1.2 \times 10^6$  in the situation of Fig. 3B in the paper.

## 1.5 Determination of the noise added by the mechanical amplifier

The noise temperature of an amplifier is determined by comparing its noise to a known noise source. Here, the noise floor which establishes the signal-to-noise ratio, is set by the effective noise temperature of the system, approximately 6...7 K.

We worked at a temperature of 30 mK, and used a weak input signal as a marker, see Fig. 4. The marker peak height versus noise floor is improved by 2.3 dB by the mechanical amplification, however, this has to be subtracted by the cavity absorption (here, -1.7 dB). We thus obtain a slight 0.6 dB improvement to the signal-to-noise ratio, which corresponds to 20 added noise quanta, matching the expectation equaling the thermal phonon number.

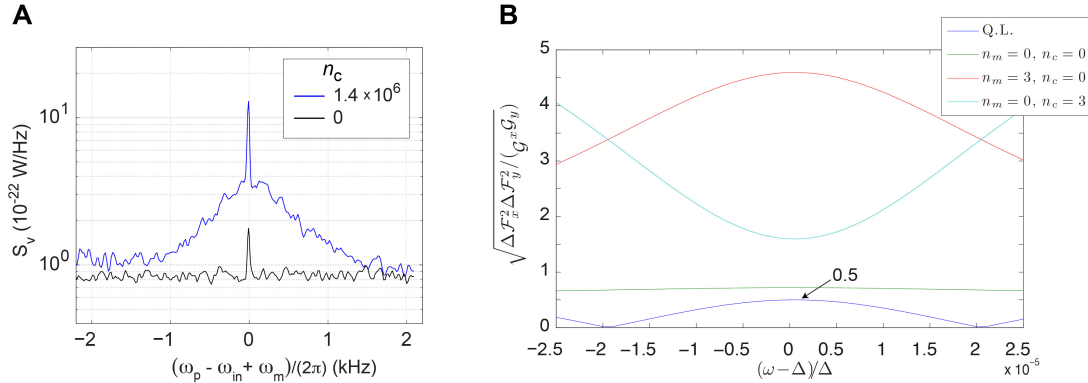


Figure 4: **Added noise of the mechanical amplifier a**, A weak probe signal (narrow peak) is employed in order to deduce signal-to-noise ratio with the amplification off (black), or on (blue).  $\Delta \simeq 0.89$ , temperature  $T = 30$  mK. The bump about the probe peak is due to the thermomechanical vibrations; **b**, theoretical plot of the added noise at the optimal value of the effective coupling for different values of  $n_m$  and  $n_c$ .

## 2 Theoretical details

### 2.1 Quantum Langevin equation for the optomechanical system

In this section we derive the dynamical equations for the cavity and the mechanical degrees of freedom for our system. After defining the Hamiltonians describing the two oscillators and the parametric coupling, we write the (non-linear) Hamilton's equations for the system. Following a standard dynamical-system approach, we separate the dynamical variables into stationary values (in the proper rotating frame) and corresponding fluctuations. In particular, the solutions of the dynamical equations for the stationary values allow to determine the value of the cavity field as a function of the pump field. These solutions set the “operating point” of the amplifier, fixing the values of the effective parameters for the fluctuations dynamics.

We now explicitly derive the quantum Langevin equations (QLE) for the optomechanical system. In absence of any coupling to the external world, the system (oscillator+cavity) Hamiltonian can be written as

$$H_{sys} = \hbar\omega_c(a_T^\dagger a_T + \frac{1}{2}) + H_{ho} + H_{int}, \quad (2)$$

where  $a_T$  is the cavity field operator, and  $\omega_c$  the cavity resonant frequency,

$$H_{ho} = \frac{p_T^2}{2m} + \frac{1}{2}m\omega_m x^2$$

is the mechanical harmonic oscillator Hamiltonian,  $m$  the mass of the mechanical system and  $\omega_m$  its resonant frequency. The Hamiltonian

$$H_{int} = -\hbar g \left( a_T^\dagger a_T + \frac{1}{2} \right) x \quad (3)$$

is the parametric interaction Hamiltonian, where  $g$  is the coupling between the mechanical degrees of freedom and the cavity. The Hamiltonian coupling the cavity with the external radiation modes can be written as

$$H_{rc}^{(I,E)} = i\hbar \int_{-\infty}^{\infty} d\omega S_{(I,E)}(\omega) \left[ b_{(I,E)}^\dagger(\omega) a_T - b_{(I,E)}(\omega) a_T^\dagger \right], \quad (4)$$

where  $s_{(I,E)}$  describes the cavity/reservoirs coupling, and the indexes  $I$ ,  $E$  refer to the external and internal baths respectively. The external bath is associated with the transmission line coupling the input and output signal with the cavity, while the internal ones refer to any other source of dissipation potentially coupling to the cavity.

The reservoir associated with the dissipative dynamics of the mechanical oscillator (hereafter mechanical bath) can be written as

$$H_{mech} = \frac{1}{2} \sum_j [(p_j - k_j x)^2 + \omega_j^2 q_j^2] \quad (5)$$

$H_{mech}$  corresponds thus to describing the reservoir in terms of a collection of independent harmonic oscillators with frequencies  $\omega_j$ , with each of which is coupled to the mechanical oscillator through  $k_j$  [4].

With the aid of the input-output formalism [5], the evolution equations for the cavity field operators, the position and momentum operators for the mechanical system can be written as

$$\dot{x} = \frac{p_T}{m} \quad (6)$$

$$\dot{p}_T = -m\omega_m^2 x + \hbar g a_T^\dagger a_T - \gamma_m p_T + \xi_T \quad (7)$$

$$\dot{a}_T = -i(\omega_c - \omega_p - gx) a_T - \frac{\gamma_c}{2} a_T - \sqrt{\gamma_I} a_{in}^I - \sqrt{\gamma_E} a_{T in}. \quad (8)$$

We have here considered a situation where the cavity is strongly driven by a coherent field oscillating at frequency  $\omega_p$ . Moreover  $\gamma_E$ ,  $\gamma_I$  represent the losses associated with the input/output port and the photon bath associated with the internal losses of the cavity ( $\gamma_c = \gamma_I + \gamma_E$ ), and  $\gamma_m$  the mechanical losses. We now linearize Eqs. (8-7), rewriting  $a_T$ ,  $x$  and  $p_T$  as the sum of a coherent field and a quantum operator

$$a_T = \alpha + a \quad (9)$$

$$x = \chi + \sqrt{\frac{\hbar}{m\omega_m}} q \quad (10)$$

$$p_T = \pi + \sqrt{\hbar m \omega_m} p. \quad (11)$$

More specifically, we have rewritten Eq. (9) with a view to the decomposition in terms of a (coherent) pump field  $\alpha_P$  and input signal and noise sources, i.e.

$$a_{Tin} = \alpha_p + a_{in}$$

Since we are interested in the steady-state solution, neglecting all fluctuations, we impose the condition  $\dot{\alpha} = \dot{\chi} = \dot{\pi} = 0$ , leading to the steady-state values (in a frame rotating at  $\omega_p$ )

$$\pi_s = 0 \tag{12}$$

$$\chi_s = \frac{\hbar g}{m\omega_m^2} \left( |\alpha_s|^2 + \frac{1}{2} \right) \tag{13}$$

$$\alpha_s = \frac{\sqrt{\gamma_E} \alpha_p}{\frac{\gamma_c}{2} + i(\omega_c - \omega_p - g\chi_s)}. \tag{14}$$

Eqs. (12, 14), can be combined into a third-order algebraic equation, leading to three stationary solutions or the cavity field  $\alpha_s$  as a function of the pump field  $\alpha_p$ .

We now focus on the solution for which  $\alpha_s \rightarrow 0$  when  $\alpha_{in} \rightarrow 0$ . In this case, the evolution equations for the fluctuation operators can be written as

$$\dot{q} = \omega_m p \tag{15}$$

$$\dot{p} = -\omega_m q - \gamma_m p + G\delta X + \xi \tag{16}$$

$$\dot{a} = i\Delta a - \frac{\gamma_c}{2} a + \frac{G}{\sqrt{2}} q + \sum_{i=I,E} \sqrt{\gamma_i} a_{in}^i \tag{17}$$

where  $\Delta = \omega_p - \omega_c - g\chi_s$ ,  $G = 2g\sqrt{\frac{\hbar}{2m\omega_m}}\alpha_s$ , having assumed, without loss of generality, that  $\alpha_s$  is real. Equations (15-17) represent the quantum Langevin equations for the cavity+mechanical resonator system. It is worth noting here that, following [6], we have not performed the rotating wave approximation for the mechanical bath degrees of freedom, this choice will affect the expression for the noise spectrum for the operator  $\xi$ .

## 2.2 Amplification

Considering the relation between input and output fields at the input/output port of the cavity [5]

$$a_{out} = \sqrt{\gamma_E} a + a_{in} \quad (18)$$

the solution of eqs. (15-17), leads to the general relating the output field to the various incoming fields

$$a_{out}(\omega) = M(\omega)a_{in}(\omega) + La_{in}^\dagger(\omega) + M_I(\omega)a_{in}^I(\omega) + L_I a_{in}^{I\dagger}(\omega) + Q(\omega)\xi(\omega) \quad (19)$$

where  $a_{in}^I(\omega)$  and  $\xi(\omega)$  represent the noise introduced by the internal losses of the cavity and the mechanical bath (see Fig.5). The power gains for the input signal ( $M$  and  $L$ ), and those for the input noise ( $M_I$ ,  $L_I$  and  $Q$ ) are given as

$$M(\omega) = \left[ \Gamma_M(\omega) \frac{\gamma_E}{\gamma_c/2 - i(\omega + \Delta)} - i \frac{\gamma_E (\Gamma_M(\omega) - 1)}{2\Delta} - 1 \right] \quad (20)$$

$$L(\omega) = -i \frac{\gamma_E (\Gamma_M(\omega) - 1)}{2\Delta} \quad (21)$$

$$M_I(\omega) = \left[ \Gamma_M(\omega) \frac{\sqrt{\gamma_E \gamma_I}}{\gamma_c/2 - i(\omega + \Delta)} - i \frac{\sqrt{\gamma_E \gamma_I} (\Gamma_M(\omega) - 1)}{2\Delta} \right] \quad (22)$$

$$L_I(\omega) = -i \frac{\sqrt{\gamma_E \gamma_I} (\Gamma_M(\omega) - 1)}{2\Delta} \quad (23)$$

$$Q(\omega) = \sqrt{\frac{\gamma_c}{2}} \frac{\Gamma_M(\omega) - 1}{\Delta G} \left[ (\Delta - \omega) - i \frac{\gamma_c}{2} \right]. \quad (24)$$

The key role in the amplification is played by the factor

$$\Gamma_M(\omega) = \frac{\omega_m^2 - \omega^2 - i\gamma_m \omega}{\omega_{\text{eff}}^2 - \omega^2 - i\gamma_{\text{eff}} \omega} \quad (25)$$

which, in turn, depends on the effective resonant frequency

$$\omega_{\text{eff}} = \left[ \omega_m^2 + \frac{G^2 \Delta \omega_m [\gamma_c^2/4 - \omega^2 + \Delta^2]}{[\gamma_c^2/4 + (\omega - \Delta)^2] [\gamma_c^2/4 + (\omega + \Delta)^2]} \right]^{1/2} \quad (26)$$

and the effective damping coefficient

$$\gamma_{\text{eff}} = \left[ \gamma_m - \frac{2\gamma_c G^2 \Delta \omega_m}{[\gamma_c^2/4 + (\omega - \Delta)^2] [\gamma_c^2/4 + (\omega + \Delta)^2]} \right] \quad (27)$$

induced by the coupling with the cavity on the mechanical resonator. At resonance  $\omega \simeq \omega_m$  and neglecting the (weak) pump dependence of  $\omega_{\text{eff}}$ , it is clear that a decrease of  $\gamma_{\text{eff}} \rightarrow 0$  will lead to  $\Gamma_M \gg 1$  (see below for stability considerations), and thus, through the  $\Gamma_M$  dependence of  $M$  and  $L$ , to an amplification of an input signal.

We use the notion of preferred quadratures [7], for which the output quadrature fields  $X_{\text{out}}$ ,  $Y_{\text{out}}$  are independent of  $Y_{\text{in}}$  and  $X_{\text{in}}$  respectively. The power gains in these quadratures are obtained as

$$\mathcal{G}_x = (|M| + |L|)^2 \quad (28)$$

$$\mathcal{G}_y = (|M| - |L|)^2 \quad (29)$$

$$\mathcal{G}_{\text{av}} = \frac{1}{2} (\mathcal{G}_x + \mathcal{G}_y) = |M|^2 + |L|^2 \quad (30)$$

The expression of the gain in the preferred quadratures corresponds to the possibility of choosing an appropriate phase for  $a_{\text{in}}$  and  $a_{\text{out}}$  leading to real-valued expressions for  $M$  and  $L$ , given by Eqs. (20, 21). In these quadratures, the amplifier equations can be written as (dropping here the added-noise terms)

$$X_{\text{out}} = (|M| + |L|) X_{\text{in}} \quad (31)$$

$$Y_{\text{out}} = (|M| - |L|) Y_{\text{in}} \quad (32)$$

$$(33)$$

thus leading to the relations given by Eqs. (28, 29) for  $\mathcal{G}_x$  and  $\mathcal{G}_y$ . In addition to the trivial difference associated with the condition  $\gamma_E \neq \gamma_I$ , reflecting different coupling mechanisms of the cavity to the external world, the expressions for  $M_I(\omega)$  and  $M(\omega)$  differ due to the

interference term appearing in the expression of  $M(\omega)$  (the third term on the right-hand side of Eq. (20)). This term represents the interference between the input (either signal or noise) that has been reflected at the cavity/transmission line interface and the input that has travelled through the cavity. The expression of the gains given by Eqs. (28-30) involve the coefficients  $M(\omega)$  and  $L(\omega)$  only, since, obviously, the signal is supposed to enter the system through the input external port only. On the other hand, while opening the cavity to the transmission line will also open that port to the noise from the transmission line, this noise is regarded as intrinsic noise of the input signal and thus does not contribute to the noise added by the amplifier. The system will thus be open to one signal source (the coherent part of  $a_{in}$ ), the noise associated with internal losses ( $a_{in}^I$ ), the noise associated with the mechanical bath ( $\xi$ ) and the noise from the transmission line (the incoherent part of  $a_{in}$ ), the latter not contributing to the noise added by the amplifier.

### 2.3 Noise: input field correlators and the quantum limit

Within this scheme, the noise added by the amplifier can be expressed in terms of noise spectra associated with the internal losses and the mechanical bath. Following a standard approach [8], the correlators for  $a_{in}$  and  $a_{in}^I$  are given by

$$\langle a_{in}^{(I)}(t)a_{in}^{(I)\dagger}(t') \rangle = [n(\omega_c) + 1] \delta(t - t') \quad (34)$$

$$\langle a_{in}^{(I)\dagger}(t)a_{in}^{(I)}(t') \rangle = n(\omega_c)\delta(t - t'). \quad (35)$$

Similarly, the mechanical noise correlator can be written as [9]

$$\langle \xi(t)\xi(t') \rangle = \int \frac{d\omega}{2\pi} \exp[-i\omega(t - t')] S_\xi(\omega) \quad (36)$$

with

$$S_\xi(\omega) = 2\gamma_m \frac{\omega}{\omega_m} \{ (n_\omega + 1)\Theta(\omega) + [(n_{-\omega} + 1)\Theta(-\omega)] \} \quad (37)$$

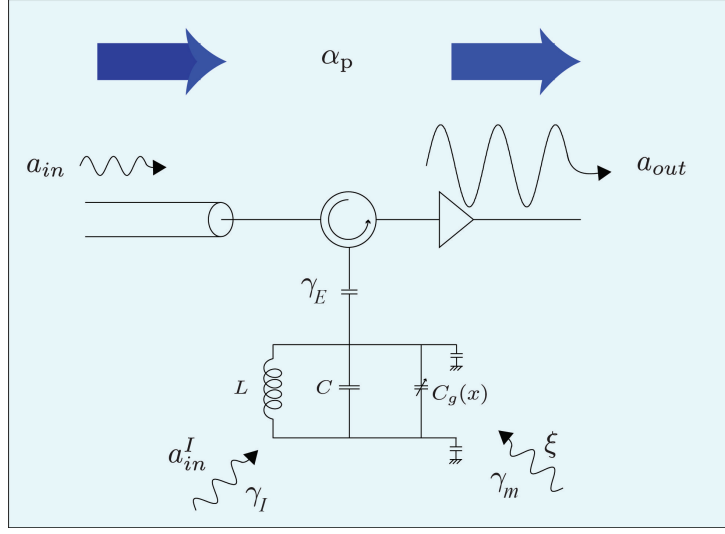


Figure 5: Schematics of the amplification scheme with an outline of the different noise sources.  $a_{in} = \alpha_{in} + \delta a_{in}$ : input field associated with the input signal  $\alpha_{in}$  and the noise at the input port  $\delta a_{in}$ .  $a_{in}^I$ : field associated with the noise reservoir acting directly on the resonant cavity.  $\xi$ : mechanical noise associated with the thermal bath.

where  $\Theta(x)$  is the Heaviside step function (see e.g. [9]). Considering a thermally populated bath, the noise spectrum assumes the form [8]

$$S_{\xi}(\omega) = \gamma_m \frac{\omega}{\omega_m} \left[ \coth \left( \frac{\hbar\omega}{kT} \right) + 1 \right] \quad (38)$$

We are now in the position to evaluate the noise added by the amplifier. We here define the operators

$$\mathcal{F}_x = \frac{1}{\sqrt{2}} \left[ M_I a_{in}^I + L_I a_{in}^{I\dagger} + Q\xi + h.c. \right] \quad (39)$$

$$\mathcal{F}_y = \frac{-i}{\sqrt{2}} \left[ M_I a_{in}^I + L_I a_{in}^{I\dagger} + Q\xi - h.c. \right] \quad (40)$$

where the appropriate phase has been included in the definition of  $M_I$ ,  $L_I$  and  $Q$  in order to satisfy the condition  $M, L \in \mathbb{R}$ .  $(\Delta\mathcal{F}_x)^2$  and  $(\Delta\mathcal{F}_y)^2$  represent the added noise by the amplifier

[7]. The condition establishing a lower bound for the added noise reads in this case

$$\sqrt{|\Delta\mathcal{F}_x|^2 |\Delta\mathcal{F}_y|^2 / (\mathcal{G}_x \mathcal{G}_y)} \geq \frac{1}{4} |1 - (\mathcal{G}_x \mathcal{G}_y)^{-1}|. \quad (41)$$

Close to the optimal effective coupling  $G_{opt} = \sqrt{\gamma_m \gamma_c}$ , and for  $\omega \simeq \omega_m$ , the expression for the added noise is given by

$$\sqrt{|\Delta\mathcal{F}_x|^2 |\Delta\mathcal{F}_y|^2 / (\mathcal{G}_x \mathcal{G}_y)} \simeq \frac{\gamma_I}{\gamma_c} (n_{opt}^I + 1/2) + \frac{\gamma_c}{\gamma_E} (n_m + 1/2). \quad (42)$$

From Eq. (42), it is possible to see that the quantum limit for the amplification can be reached in absence of internal cavity losses and for a zero-temperature mechanical reservoir. In our experimental setup  $n_{opt}^I \simeq 0$ , leading to a linear increase of the added noise with the number of mechanical reservoir phonons. The linear dependence coefficient is given by the ratio between total and external losses.

## 2.4 Stability and validity of the linearized model

In obtaining the QLE for the cavity and the mechanical resonator, we have linearized the equations of motion for the cavity+mechanical resonator system. We will here discuss the criterion for the stability and the limits of validity of the (linear) QLE equations considered to analyze the system dynamics (Ginsburg criterion) [10]. The requirement for the system stability is that the poles of the effective mechanical susceptibility, induced by the coupling between the mechanical resonator and the cavity, lie in the lower complex half-plane. In other terms, the effective mechanical damping  $\gamma_{\text{eff}}$  must be positive in order for the system to be stable. The condition  $\gamma_{\text{eff}} \rightarrow 0^+$  correspond to the situation of maximal gain and, on crossing the  $\gamma_{\text{eff}} = 0$  value, to the loss of stability. In the linearization procedure we have assumed that the term  $x \cdot a_T$  appearing in Eq. (8) could be expanded as

$$(\xi + q) \cdot (\alpha + a) \simeq \xi\alpha + \alpha q + \xi a \quad (43)$$

analogously,

$$a_T^\dagger a_T \simeq \alpha^2 + \alpha^* a + \alpha a^\dagger. \quad (44)$$

Eqs. (43) and (44) thus establish that, for the linearized QLE equations to aptly describe the dynamics of the optomechanical system, the following conditons must be met

$$\frac{\langle qa \rangle}{\alpha_s \chi_s} \ll 1 \quad (45)$$

$$\frac{\langle a^\dagger a \rangle}{\alpha_s^2} \ll 1, \quad (46)$$

The solutions for  $q$  and  $a$  of the QLE as a function of the input field  $a_{in}$  lead to the following condition for the ratio between the signal and the pump power

$$\frac{\langle a_{in}^\dagger a_{in} \rangle}{\alpha_s^2} \ll \frac{1}{|\Gamma_M|^2}. \quad (47)$$

It is thus clear from Eq. (47) that for large enough values of  $|\Gamma_M|$ , the linearized description of the system physics breaks down. However as it can be seen from Fig. 6, there is a large range of parameters where, while having a gain significantly larger than 1, the linear model is still valid.

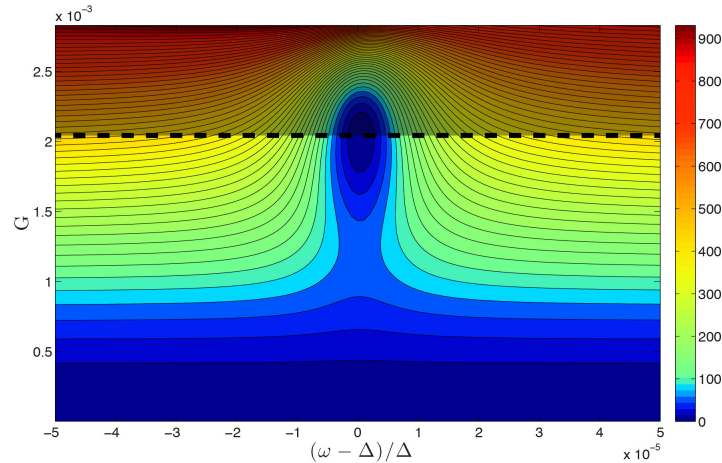


Figure 6: Number of signal photons ensuring the validity of the linear-regime analysis as a function of  $\omega$  and  $G$ . We have assumed  $\left(\langle a_{in}^\dagger a_{in} \rangle / \alpha_s^2\right)_{\text{threshold}} = 10^{-4} / |\Gamma_M|^2$

## References

- [1] Sulkko, J. *et al.* Strong Gate Coupling of High-Q Nanomechanical Resonators. *Nano Lett.* **10**, 4884–4889 (2010).
- [2] Teufel, J. D., Harlow, J. W. & Regal, C. A. Dynamical backaction of microwave fields on a nanomechanical oscillator. *Phys. Rev. Lett.* (2008).
- [3] Rocheleau, T. *et al.* Preparation and detection of a mechanical resonator near the ground state of motion. *Nature* **463**, 72–75 (2010).
- [4] Caldeira, A. & Leggett, A. Influence of Dissipation on Quantum Tunneling in Macroscopic Systems. *Phys. Rev. Lett.* **46**, 211–214 (1981).
- [5] Walls, D. F. & Milburn, G. J. *Quantum Optics* (Springer, Berlin, 2007).
- [6] Giovannetti, V. & Vitali, D. Phase-noise measurement in a cavity with a movable mirror undergoing quantum Brownian motion. *Phys. Rev. A* **63**, 023812 (2001).
- [7] Caves, C. M. Quantum limits on noise in linear-amplifiers. *Phys. Rev. D* **26**, 1817–1839 (1982).
- [8] Genes, C., Vitali, D., Tombesi, P., Gigan, S. & Aspelmeyer, M. Ground-state cooling of a micromechanical oscillator: Comparing cold damping and cavity-assisted cooling schemes. *Phys. Rev. A* **77**, 033804 (2008).
- [9] Clerk, A. A., Devoret, M. H., Girvin, S. M., Marquardt, F. & Schoelkopf, R. J. Introduction to quantum noise, measurement, and amplification. *Rev. Mod. Phys.* **82**, 1155–1208 (2010).

- [10] Mancini, S. & Tombesi, P. Quantum-noise reduction by radiation pressure. *Phys. Rev. A* **49**, 4055–4065 (1994).